



# Silver Nanoparticles for Colorimetric Dual Ion Sensing and Development of Paper Sensors: A Strategy Towards Waste Valorisation and Sustainability

Rugmini R.<sup>1</sup> · B. D. Sri Chandana<sup>1</sup> · K. C. Sekhar<sup>1</sup>

Received: 4 June 2024 / Accepted: 15 July 2024

© The Author(s), under exclusive licence to Springer Science+Business Media, LLC, part of Springer Nature 2024

## Abstract

Iron and copper are essential for all living organisms, and their balance is crucial as both deficiency and excess can cause health problems. Therefore, this study presents a colorimetric method for detecting  $\text{Fe}^{3+}$  and  $\text{Cu}^{2+}$  ions in aqueous samples using silver nanoparticles (AgNPs) synthesised from *Ocimum sanctum* (Tulasi) leaf extract (TLE). It is observed that AgNPs show optimum plasmonic properties at a precursor-leaf extract ratio of 1:5, reaction temperature of 60 °C and reaction time of 2 h. The AgNPs exhibit the face-centred cubic (fcc) structure and show a surface plasmon resonance peak at 413 nm, hydrodynamic size of  $18 \pm 5$  nm, zeta potential of  $-25.5$  mV and particle size of 57 nm. FTIR spectra confirm the stabilisation of AgNPs. It is worthy to note that, AgNPs exhibit selective detection of  $\text{Fe}^{3+}$  and  $\text{Cu}^{2+}$  over other metal ions and the detection mechanism is proposed based on the reduction potential values. The quantitative detection range for  $\text{Fe}^{3+}$  and  $\text{Cu}^{2+}$  are found to be 0–800  $\mu\text{M}$  and 0–600  $\mu\text{M}$ , with the detection limits of 9.1  $\mu\text{M}$  and 19.5  $\mu\text{M}$ , respectively. Additionally, AgNP-based paper sensors for  $\text{Cu}^{2+}$  detection show qualitative and quantitative colorimetric performance with a detection limit of 23.1  $\mu\text{M}$ . These findings suggest that both AgNPs solution and AgNP-based paper sensors are the potential candidates for metal ion detection.

**Keywords** Silver nanoparticles · Green synthesis · Optical sensing · Dual ion detection · Paper sensors

## Introduction

Transition metals like Mn, Fe, Co, Cu and Zn are crucial in biological systems due to their roles in protein binding and enzymatic reactions that are essential for metabolism [1–4]. Iron (Fe) and copper (Cu) are especially important due to their involvement in various activities from cellular functions to oceanic biogeochemical cycles. Fe aids in electron transport, oxygen transport, energy metabolism, neurotransmission, DNA/RNA/protein synthesis and brain functions, whilst Cu is vital for mitochondrial respiration, brain development, blood vessel and tissue formation, neurotransmission and cancer cell destruction [5–8]. Proper intake and regulation of these ions are essential, as excess amounts

can cause cellular damage, organ dysfunction, neurological diseases, movement disorders and cancer [4, 9]. Therefore, developing simple and cost-effective methods for selective detection of Fe and Cu in blood, tissues and environmental water samples is essential. This is challenging due to their complex biological roles, similar redox properties and the unique interferences in different environments.

There are number of detection methods for Fe and Cu content in aqueous samples including atomic absorption spectrometry, inductively coupled plasma-optical emission spectrometry, electrochemical methods like voltammetry and potentiometry, fluorescence quenching methods etc. [10, 11]. But these methods require specific laboratory conditions, sophisticated instruments and trained technical or procedural assistance to perform the detection. Notably, optical detection, particularly using paper-based colorimetric sensors, stands out for several reasons. Unlike the traditional methods like electrochemical sensing, which often requires precise electrode preparation, stable power sources and careful calibration, colorimetric sensors offer straightforward visual interpretation without the need for complex

✉ K. C. Sekhar  
sekhar.koppole@gmail.com

<sup>1</sup> Department of Physics, School of Basic and Applied Sciences, Central University of Tamil Nadu, 610005 Thiruvavur, India

equipment. This ease of use makes them accessible to non-specialists and suitable for field applications. In this context, metal nanoparticles (MNPs), due to their unique properties like surface plasmon resonance (SPR), high chemical and thermal stability, easy synthesis and storage, are widely investigated for the selective and sensitive detection of various heavy metal ions [12–14]. Amongst MNPs, silver nanoparticles (AgNPs) are ideal for sensor fabrication due to their strong SPR absorption in the visible region, controllable size and tunable optical properties, enabling naked-eye detection with minimal precursor [15–18]. For instance, AgNPs are successfully employed as a sensor towards the colorimetric detection of  $\text{Hg}^{2+}$  ions and achieved a limit of detection of 3.25 nM within a very short span of 3 min [19]. However, there are only few investigations where AgNPs are employed for the colorimetric detection of  $\text{Fe}^{3+}$  and  $\text{Cu}^{2+}$  ions [11, 20, 21]. It is noteworthy that Doan et al. recently reported a selective and sensitive colorimetric detection of  $\text{Fe}^{3+}$  using AgNPs and achieved a detection limit of 1.5  $\mu\text{M}$  [22]. With regard to paper sensors for  $\text{Cu}^{2+}$  detection, one of the appreciable works is by Ratnarathorn et al., in which a detection limit of 7.8 nM was achieved by homocysteine and dithiothreitol modified AgNPs [23].

Nevertheless, approximately 70% of reported probes are chemically synthesised, raising environmental concerns, especially when detecting analytes in food samples or body fluids due to potential chemical interactions [18, 20, 24–26]. Green synthesis of AgNPs is an effective strategy to address these challenges [27–29]. *Ocimum sanctum*, commonly known as *Tulasi*, apart from its highly acclaimed antimicrobial effect, is an efficient reducing and stabilising agent which is employed for the green synthesis of AgNPs [30, 31]. Tulasi leaves contain various compounds, notably polyphenols, which have a higher affinity for iron, a lower affinity for copper, and minimal affinity for other metals [32, 33]. The antimicrobial properties of Tulasi enhance the robustness of the sensing platform by preventing biological interferences. This unique combination makes Tulasi leaf extract highly effective for developing selective, efficient and contamination-resistant detection methods for iron and copper.

Therefore, this study introduces a novel approach for dual ion sensing using AgNPs synthesised with Tulasi leaf extract. The optimization of synthesis parameters ensures superior sensing performance in terms of both detection limit and range. Additionally, an innovative and sustainable concept is proposed through the fabrication of AgNP-based paper sensors, which are flexible, easy to use, portable and cost-effective. Waste valorisation is explored by utilising paper waste from hole punches, thereby simplifying the detection process and enhancing environmental sustainability. This method not only provides an efficient and eco-friendly solution but also leverages readily available

materials, reducing costs and promoting green chemistry. Overall, this work represents a significant advancement in the field of metal ion detection, combining environmental benefits with practical applications.

## Materials and Methods

### Preparation of Tulasi Leaf Extract (TLE)

The Tulasi leaf extract (TLE) is prepared as follows. First, Tulasi leaves collected from the premises of Central University of Tamil Nadu, India, were washed and dried at room temperature. Then, 15 g of dried Tulasi leaves were weighed and immersed in 200 mL de-ionised (DI) water, stirred for 3 h with 800 rpm at a temperature of 60 °C. The mixture was cooled to room temperature and filtered with Whatman filter paper. The filtered extract was stored in refrigerator for further use [34].

### Preparation of Precursor Solution

0.1 M  $\text{AgNO}_3$  solution was prepared by dissolving 0.169 g of  $\text{AgNO}_3$  ( $\geq 99\%$ , Fisher Scientific) salt in 10 mL of DI water by stirring at 1000 rpm for 15 min at room temperature.

### Synthesis and Optimisation of AgNPs

The volume of precursor solution (P), i.e.,  $\text{AgNO}_3$  to volume of Tulasi leaf extract (E) is varied for the optimization of AgNPs. For instance, 10  $\mu\text{L}$  of 0.1 M  $\text{AgNO}_3$  solution and the same volume of TLE were dissolved in 20 mL DI water and stirred for 30 min with 500 rpm at room temperature to prepare the AgNPs with precursor-extract (P-E) ratio of 1:1. The same procedure is repeated with 10  $\mu\text{L}$   $\text{AgNO}_3$  solution and varying the volume of TLE to 20, 30, 40 and 50  $\mu\text{L}$  to obtain the AgNPs with P-E ratios of 1:2, 1:3, 1:4 and 1:5 respectively. To study the effect of reaction time, AgNPs with P-E ratio of 1:5 was prepared under the above-mentioned conditions and the UV–visible spectra was taken at equal time intervals of 10 min. Furthermore, to study the effect of reaction temperature, the synthesis was repeated by varying the temperature from room temperature ( $\text{RT} = 30\text{ }^\circ\text{C}$ ) to 40, 50, 60, 70 and 80 °C. After 2 h of heat treatment, the UV–visible spectrum was taken for all the samples.

### Characterisations

The Fourier transform infra-red (FTIR) spectra of TLE and the optimised AgNPs were taken using PerkinElmer spectrum 2 spectrometer in the wavenumber range 400 to 4000  $\text{cm}^{-1}$ . Shimadzu UV-1800 spectrophotometer was

employed to measure the UV–visible absorbance of AgNPs in the range 200–900 nm. The dynamic light scattering (DLS) and zeta potential (ZP) measurements were performed using Malvern Zeta Sizer Nano ZSP. The scanning electron microscopy (SEM) and energy dispersive X-ray spectrum (EDS) were obtained by JEOL-JSM-IT-200 and the X-ray diffraction pattern was obtained by Malvern Panalytical Empyrean X-ray diffractometer.

## Sensing

Ten-millimolar stock solutions of  $\text{Cu}^{2+}$ ,  $\text{Fe}^{3+}$ ,  $\text{K}^+$ ,  $\text{Mg}^{2+}$ ,  $\text{Sr}^{2+}$ ,  $\text{Mn}^{2+}$ ,  $\text{Ni}^{2+}$ ,  $\text{Sb}^{3+}$ ,  $\text{As}^{3+}$ ,  $\text{Hg}^{2+}$ ,  $\text{Fe}^{2+}$ ,  $\text{Co}^{2+}$ ,  $\text{Ba}^{2+}$  and  $\text{Ca}^{2+}$  are prepared using the respective chloride, carbonate, sulphate and oxide compounds of the ions ( $\geq 98\%$ , Merck, India). Two millilitres of AgNPs were taken in separate vials and to each vial, 0.1 mL of the stock solution is added and shaken well. A photograph is taken after 10 min of contact time and further UV–visible spectrum is recorded.

Ten-millimolar stock solutions of  $\text{Fe}^{3+}$  and  $\text{Cu}^{2+}$  are diluted to prepare various concentrations of both the ions from 10 to 800  $\mu\text{M}$ . 1 mL of each concentration is mixed with 1 mL of AgNPs and the absorption spectra are taken. DLS and ZP measurements are done for specified concentrations to analyse the trend in the hydrodynamic size and to support the mechanism.

## Fabrication of Paper Sensors

White coloured paper discs from the hole punch were collected and 20 of them were spread to a petri-dish to which 2 mL of AgNPs were added. The paper punches were completely immersed in the AgNPs and were heated at 60 °C until get dried and cooled to room temperature naturally. Twenty microlitres of  $\text{Cu}^{2+}$  stock solutions with different concentrations were dropped onto the paper sensors one by one and then allowed them to dry naturally at room temperature for 4 h. The colour of each sensor was analysed using *Adobe photoshop* for quantification.

## Results and Discussions

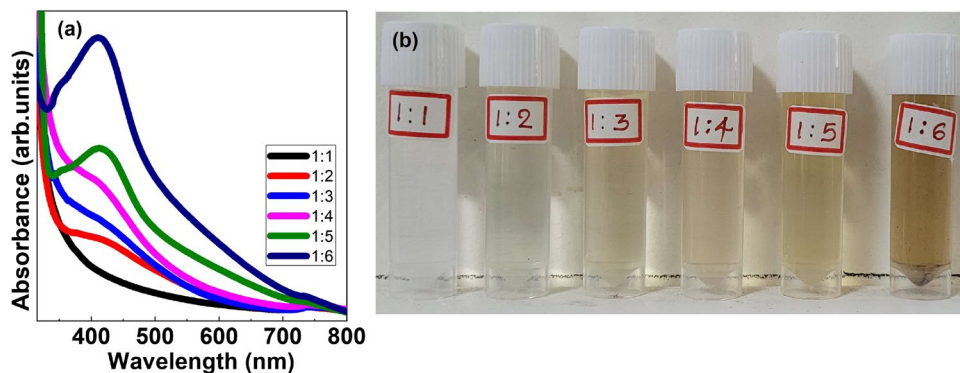
### Effect of P-E Ratio

Figure 1a shows the absorption spectra of the AgNPs synthesised with varying amounts of leaf extract. It can be observed that the formation of AgNPs does not happen for P-E ratio of 1:1 at room temperature. This suggests that the amount of leaf extract is not sufficient for the reduction of  $\text{Ag}^+$  ions. As the amount of extract increases from 1:1 to 1:2, 1:3 and 1:4, the intensity increases and a shoulder peak starts to appear in the range 400 nm to 450 nm, indicating the formation of AgNPs. When the precursor-extract ratio reaches to 1:5, a significant SPR peak around 450 nm is observed. As the ratio is increased to 1:6, along with the SPR peak at around 450 nm, another prominent peak appears at around 350 nm, which corresponds to the TLE. In addition, a gradual colour change from colourless to pale yellow and brownish yellow was observed as the ratio is increased as seen in Fig. 1b. Thus, the formation of AgNPs and increase in absorbance with the addition of leaf extract can be attributed to the inclusion of more and more reducing components like quercetin, flavonoids, terpenoids and phenolic compounds present in Tulasi which can actively participate in the reduction of  $\text{Ag}^+$  ions into AgNPs [35]. Hence, as TLE is increased, more ions are reduced and the intensity of SPR band increases. However, the presence of TLE peak at 1:6 ratio suggests that, there is an excess of leaf content. The prominent SPR peak at the P-E ratio of 1:5 indicates that the amount of leaf is sufficient enough to reduce the ions present in the solution. Hence, to avoid excess amounts of leaf and its effects, 1:5 ratio was chosen as the optimum P-E ratio for further investigations.

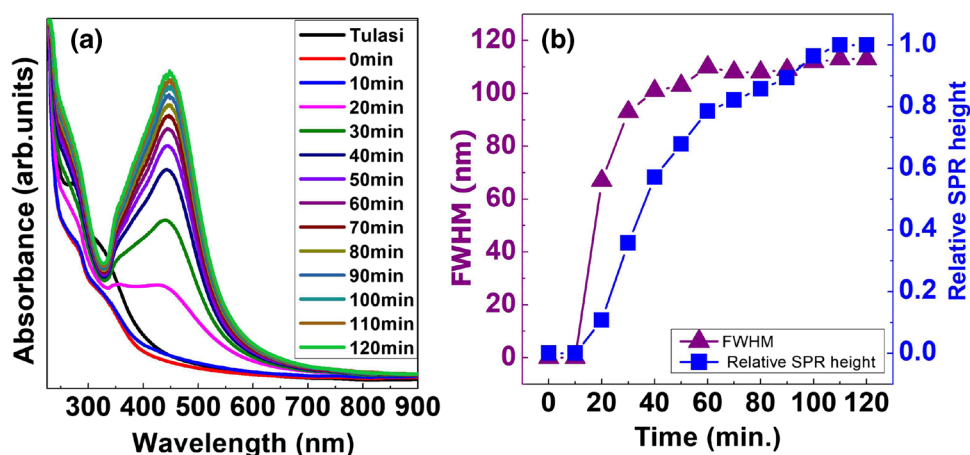
### Effect of Reaction Time

The UV–visible spectra of the AgNPs at regular intervals of time during the synthesis is given in Fig. 2a. It is observed that initially, there were only two peaks at 273 nm

**Fig. 1** a Absorption spectra and b images of AgNPs synthesised with different P-E ratio



**Fig. 2** The effect of reaction time on **a** absorption spectra of AgNPs and **b** FWHM and relative SPR peak height



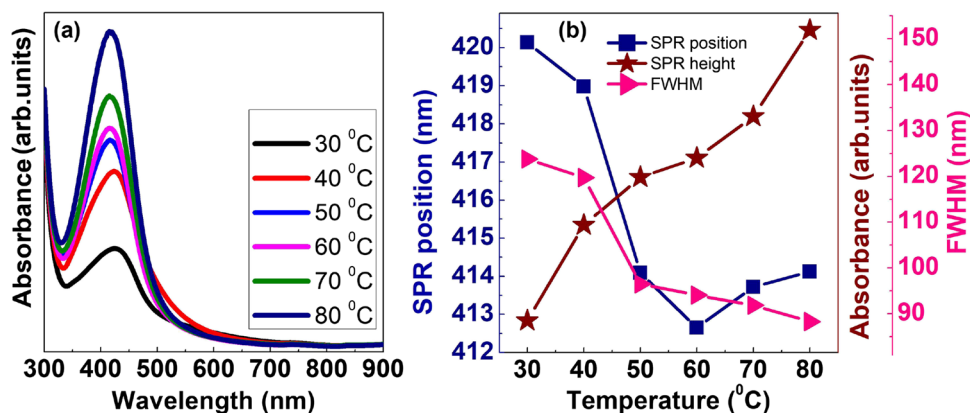
and 325 nm which corresponds to Tulasi leaf extract. As time increases from 0 to 20 min., a small peak at 438 nm starts to appear which indicates the formation of AgNPs as AgNPs have their characteristic SPR absorption peak in the region 400–450 nm [30]. Furthermore, the height of this peak increases with time indicating that more and more  $\text{Ag}^+$  ions are getting reduced and stabilised by Tulasi leaf extract as time increases. The variation of relative SPR peak height and FWHM with time is shown in Fig. 2b. It is observed that more than 78% of the maximum absorbance is reached within the first 60 min, and as the time increases to 120 min., the absorbance gradually reaches the maximum value. This can be considered a merit of the synthesis method since green synthesis methods are usually reported as more time consuming as the typical reaction time can extend from 6 h to even 24 h [36]. The FWHM shows a rapid increase from 0 to 100 nm within the first 40 min which can be considered the initial stage of formation of AgNPs. Then, there is only a slight increase in FWHM up to 12% until the process completes. This suggests that the homogeneity of the cluster size is preserved until the end of the process and the sharp peak obtained indicates the stability of the AgNPs. Moreover

since there is no shift in the SPR position, it can be confirmed that there is no change in the size of the particles [37]. Hence, 2 h is chosen as the optimum reaction time.

### Effect of Reaction Temperature

Figure 3a shows the absorption spectra of AgNPs synthesised at different temperatures with a P-E ratio of 1:5 and Fig. 3b shows the variation of SPR intensity, SPR position and FWHM with temperature. More and more intense and sharper SPR peaks are obtained as the reaction temperature is increased from 30 to 80 °C. SPR position shows a blue shift up to 60 °C and then shifts to longer wavelength at higher temperatures. These observations can be explained on the basis of dependence of nucleation and growth rate on higher reaction temperatures [38]. A high reaction temperature increases the rate of nucleation and hence smaller particles are formed. This introduces the blue shift in SPR position. Furthermore, as temperature rises the number of smaller particles increases due to increased reduction rate. Subsequently the uniformity of size distribution is achieved which results in higher SPR

**Fig. 3** **a** Absorption spectra of AgNPs and **b** SPR position, FWHM and relative SPR height with varying reaction temperature



intensity and lower FWHM respectively [35]. But at a higher temperature, the growth rate is also higher. This increases the cluster size, and hence, after 60 °C, there is a red shift of SPR position even though the intensity is increased due to higher reduction rate [39]. It is clear that, beyond 60 °C, the changes in the FWHM and SPR position are very low which indicates that there is only slight variation in the size of the particles beyond 60 °C, but the number of uniform-sized particles is increased. Considering the stability of smaller particles and energy minimization, 60 °C is chosen as the optimum reaction temperature and this is in good agreement with the literature [40].

### FTIR Spectroscopy

To confirm the stabilisation of AgNPs by TLE, the FTIR spectroscopy was performed. Figure 4 shows the FTIR spectra of TLE and the optimised AgNPs. Three major peaks observed in the leaf extract are at 1634, 2120 and around 3300  $\text{cm}^{-1}$  which correspond to the C=O stretching of amide groups, stretching of alkynes and stretching of O–H groups respectively. These arise from the phenolic and alcoholic contents of the flavonoids, terpenoids and the amides of proteins present in the leaf extract [41]. There is no significant variations taken place in the IR bands of leaf extract after the synthesis of AgNPs. The presence of these unaltered structures containing negative charge in the AgNPs ensures the stability of the colloid and the results are in good agreement with the previous literature [42].

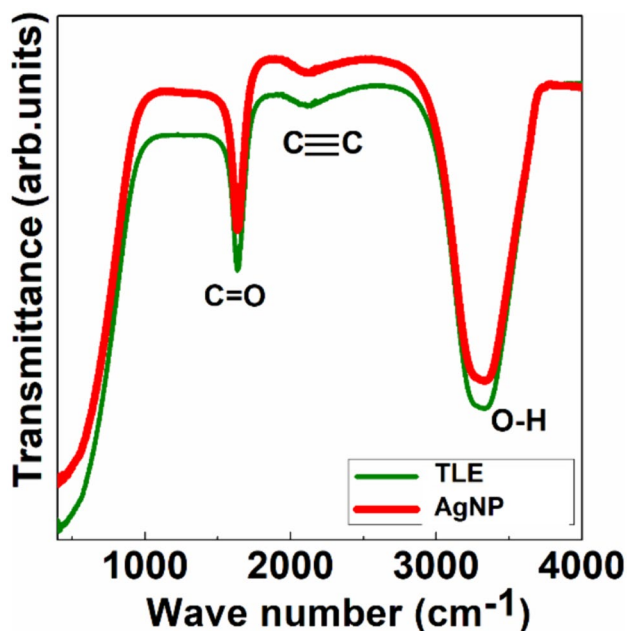


Fig. 4 FTIR spectra of TLE and AgNPs

### Microstructure of AgNPs

The X-ray diffraction (XRD) pattern of optimised AgNPs is shown in Fig. 5a and all the reflections were indexed according to JCPDS file no: 00–004–0783. The presence of (110), (220), (311) and (222) planes indicates the face-centred cubic lattice of AgNPs. The SEM image of the AgNPs is shown in Fig. 5b. An enlarged view of the same image and the size distribution of the AgNPs are shown in the inset of Fig. 5b. The average size was obtained as 57 nm which strongly aligns with the optical properties of the AgNPs. In a recent investigation by Jaffar et al., it was reported that the green synthesised AgNPs of size around 50 nm exhibit SPR absorbance at around 420 nm. This supports the results presented in this work [43]. The energy dispersive X-ray spectrum (EDS) as shown in Fig. 5c confirms the formation of AgNPs with the presence of peak at around 3.0 keV. The presence of carbon and oxygen could be obtained from TLE which contain plenty of organic functional groups like flavonoids, terpenoids etc. having both these elements [33].

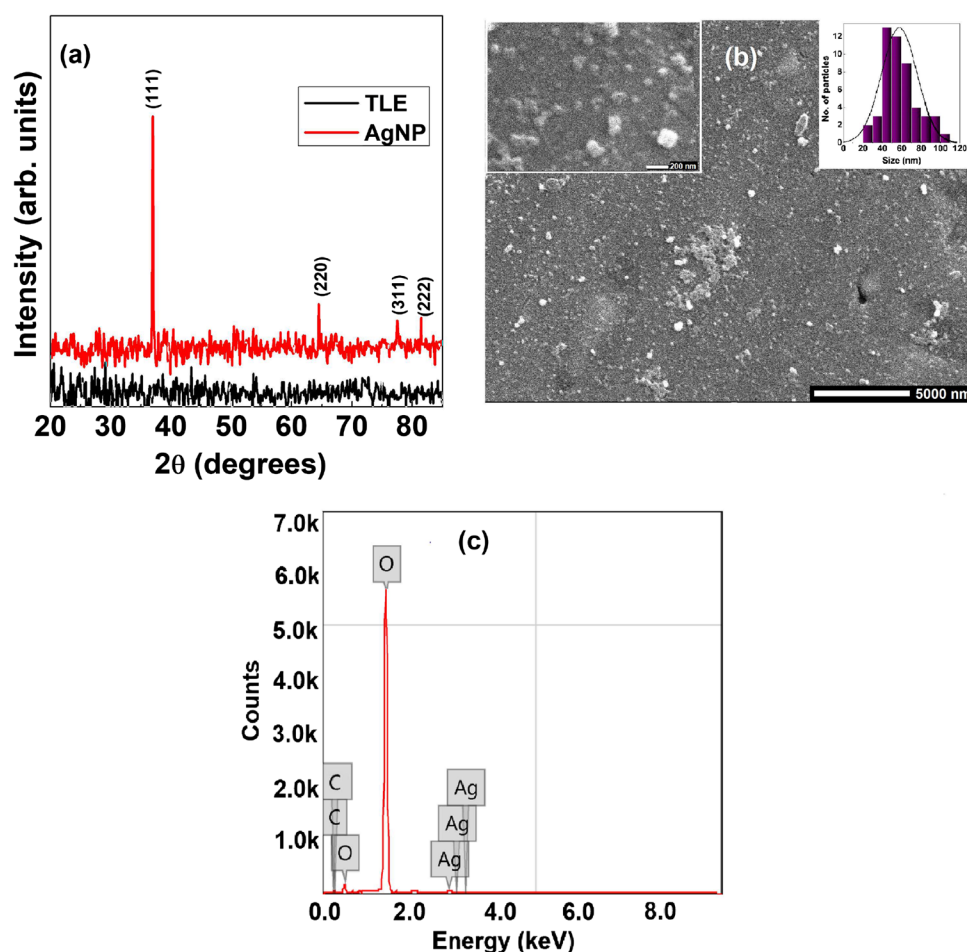
### Dynamic Light Scattering (DLS) Spectroscopy

Figure 6 shows the size measurement of the synthesised AgNPs using DLS spectroscopy. The number versus diameter curve shows the distribution centred at  $18 \pm 5$  nm. The polydispersity index (PDI) of the sample is obtained as 0.409, which indicates the monodispersed AgNPs in the colloid. There is a profound dependence of size of the NPs on the position of SPR spectrum. The results obtained in this work are in good agreement with the reported synthesis of AgNPs using Tulasi leaf extract [42].

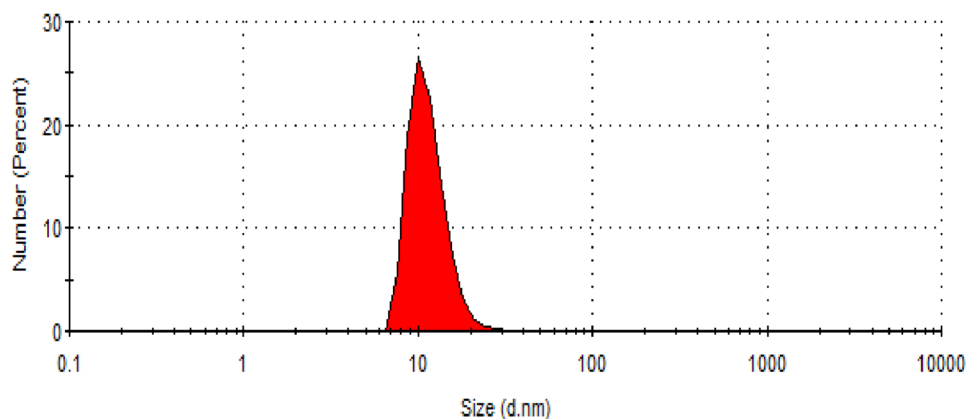
### Zeta Potential

Figure 7 shows the zeta potential of AgNPs synthesised at optimum conditions. The whole distribution curve appears in the negative potential quadrant, extends to  $-50$  mV and is centred at  $-25.5$  mV. Gumustas et al. reported that the zeta potential magnitude less than 5 mV for a colloid can lead to agglomeration [44]. The zeta potential magnitude of as-synthesised AgNPs is several folds greater than the threshold value which ensures a high stability of the synthesised NPs. The sharp negative value indicates that the AgNPs are effectively capped by the negatively charged species like hydroxyl and carboxylic acid groups present in the leaf extract. The electrostatic repulsion arising from this negative surface potential enables the AgNPs to counter the van der Waals forces and thereby, to prevent agglomeration. Moreover, the zeta potential value obtained in this work is

**Fig. 5** **a** XRD pattern, **b** SEM image with enlarged view and size distribution (insets), and **c** EDS of AgNPs



**Fig. 6** Number distribution of AgNPs as a function of their diameter



better when compared to that of previously reported green synthesised AgNPs [45–47].

### Detection of Fe<sup>3+</sup> and Cu<sup>2+</sup> Ions

Figure 8 shows the photographs AgNPs treated with the stock solutions of different ions along with the blank solution. It can be clearly observed with naked eyes that there

is a colour change only for AgNPs treated with the solution containing Fe<sup>3+</sup> and Cu<sup>2+</sup> ions. The solutions containing all other ions do not alter the colour, brownish red, of the blank solution placed at the right end whereas Fe<sup>3+</sup> changes it to pale yellow and Cu<sup>2+</sup> turns it colourless. This can be used to qualitatively detect Fe<sup>3+</sup> and Cu<sup>2+</sup> ions selectively from other ions present in aqueous samples.

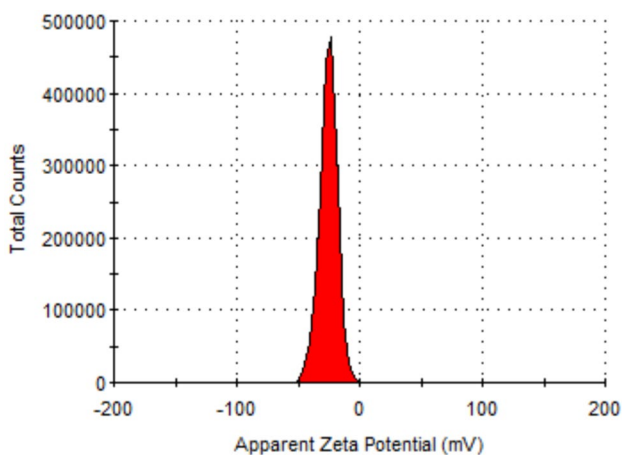


Fig. 7 Zeta potential of AgNPs

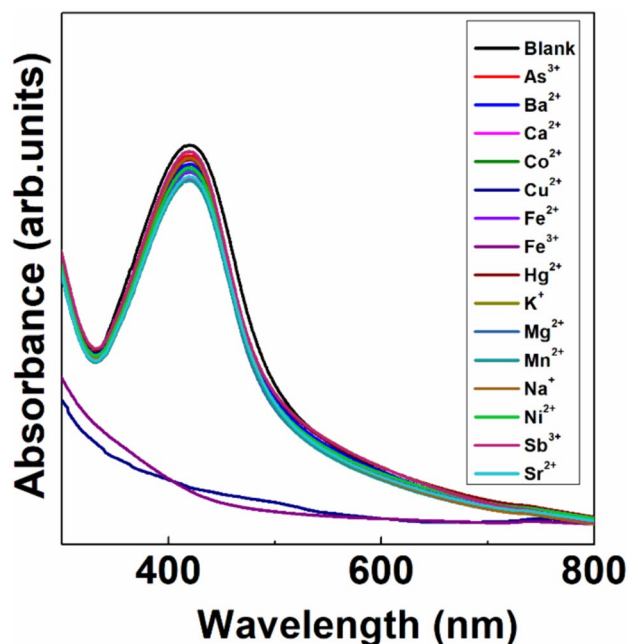


Fig. 9 Absorption spectra of AgNP solutions treated with different metal ions

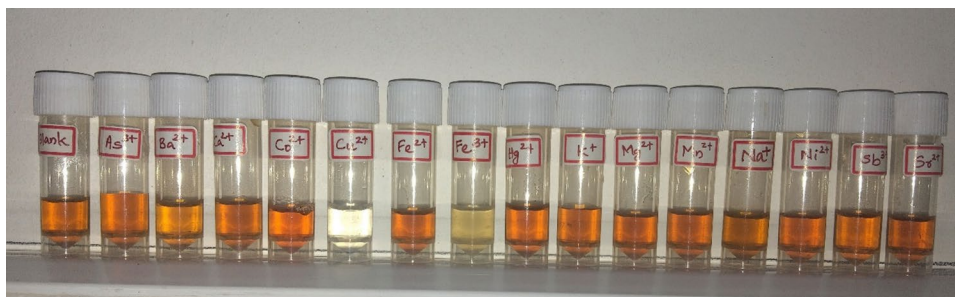
### Spectroscopic Analysis

To quantify the efficiency of detection, the absorption spectra of all these solutions are recorded and shown in Fig. 9. It is clear that the solutions having all ions but Fe<sup>3+</sup> and Cu<sup>2+</sup> show no variation in the absorption spectra from that of AgNPs. The characteristic features of SPR band like intensity, position and FWHM are not affected by the ions which suggests that the stability of AgNPs are not lost due to the introduction of these ions. However, AgNPs treated with Fe<sup>3+</sup> (AgNP-Fe) and Cu<sup>2+</sup> (AgNP-Cu) shows a remarkable variation in the absorbance. Both the AgNP-Fe and AgNP-Cu show no absorption peak in the SPR range of AgNPs which reveals that the stability of AgNPs is completely lost due to the introduction of these ions.

This can be explained using the relative reduction potentials of the ions. The standard reduction potentials (in volts) of the reactions involving the above mentioned ions are shown below [48, 49]



Fig. 8 Images of AgNP solutions treated with different metal ions



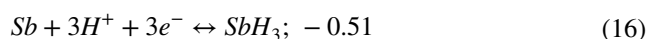


**Table 1** Cell potentials of different metals with Ag

System	Cell potential (V)
Ag-As <sup>3+</sup>	-2.12
Ag-Ba <sup>2+</sup>	-4.49
Ag-Ca <sup>2+</sup>	-4.45
Ag-Co <sup>2+</sup>	-1.857
<b>Ag-Cu<sup>2+</sup></b>	<b>-0.22</b>
Ag-Fe <sup>2+</sup>	-2.02
<b>Ag-Fe<sup>3+</sup></b>	<b>-0.02</b>
Ag-Hg	-0.73
Ag-K <sup>+</sup>	-3.72
Ag-Mn <sup>2+</sup>	-2.76
Ag-Mg <sup>2+</sup>	-4.28
Ag-Na <sup>+</sup>	-3.50
Ag-Ni <sup>2+</sup>	-1.84
Ag-Sb <sup>3+</sup>	-2.88
Ag-Sr <sup>2+</sup>	-4.48

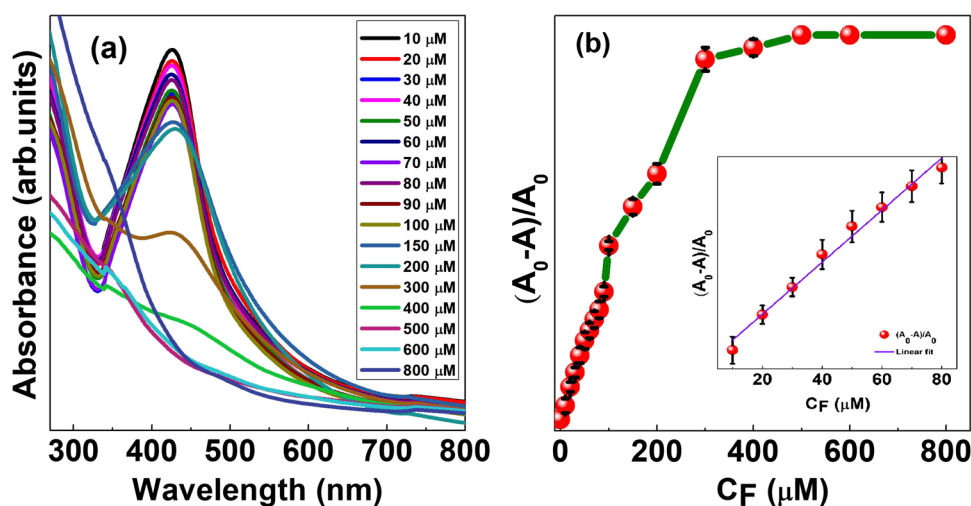
Considering the reduction potentials of the half reactions, the cell potentials of Ag with each of the above ions are calculated and presented in Table 1 [50].

The reactions having positive cell potentials takes place spontaneously. As the negative magnitude of cell potential increases, more external energy is needed for the reaction to take place. Analysing Table 1, it is clear that no other ions except Fe<sup>3+</sup> and Cu<sup>2+</sup> have the ability to oxidise Ag spontaneously since their cell potentials with Ag are highly negative. On the other hand, Fe<sup>3+</sup> and Cu<sup>2+</sup> having a slight negative potential value can oxidise Ag at an expense of very feeble external energy. Zou et al. reported that the presence of chloride ions can reduce the potential of metal ions in aqueous solutions. The decrease in reduction potential of ions like Fe<sup>3+</sup> and Cu<sup>2+</sup> is much larger when compared with other noble metal ions like Ag<sup>+</sup> or Au<sup>+</sup> [51]. Similarly, oxidation of Ag by Fe<sup>3+</sup> and Cu<sup>2+</sup> takes place due to the presence of chloride ions provided by the salt solution as a result of decrease in the reduction potential of Ag/Ag<sup>+</sup>. This collapse the stability of AgNPs and makes the solution colourless.

### Quantitative Detection of Fe<sup>3+</sup>

Figure 10a shows the absorption spectra of AgNPs treated with varying amounts of Fe<sup>3+</sup> ion solutions. It is observed that there is a decrease in the intensity of SPR peak with increase in the concentration of Fe<sup>3+</sup> (C<sub>F</sub>). For the initial concentrations, there is a gradual decrease in the SPR intensity, and as the C<sub>F</sub> exceeds 200 μM, there is a sudden fall in the SPR intensity. The SPR position shows negligible variations up to 200 μM, and for higher C<sub>F</sub>, there is a red shift. Figure 10b shows the relative variation of change in absorbance (ΔA = A<sub>0</sub> - A) with respect to the initial absorbance (A<sub>0</sub>) as a function of C<sub>F</sub>. Though the plot is non-linear in the entire concentration range, ΔA/A<sub>0</sub> varies linearly with C<sub>F</sub> in

**Fig. 10** **a** Absorption spectra of AgNPs treated with different concentrations of Fe<sup>3+</sup> in μM and **b** relative change in absorbance as a function of C<sub>F</sub>. (Linear fit of the experimental data for lower concentrations is included in the inset)





the lower concentration range which is enlarged and shown in the inset. A linear fit satisfying Eq. (17) was obtained with  $R^2 = 0.99$  which indicates a smooth convergence of the experimental data.

$$\Delta A/A_0 = 0.003C_F + 0.013 \quad (17)$$

The limit of detection (LOD) is calculated using the expression (18)

$$LOD = 3.3\sigma/s \quad (18)$$

And, the limit of quantification (LOQ) is calculated using the expression (19)

$$LOQ = 10\sigma/s \quad (19)$$

where  $\sigma$  is the standard deviation and  $s$  is the slope of the linear fit. The calculated value of LOD is  $9.1 \mu\text{M}$  and LOQ is  $26.6 \mu\text{M}$  which is significantly better compared with the previous sensing probes [52–54].

The practical application of the AgNP sensor was verified by testing real samples such as drinking water, tap water and pond water spiked with known concentration of  $\text{Fe}^{3+}$  and the results are shown in Fig. 11

All the samples are spiked with  $20 \mu\text{M}$  of  $\text{Fe}^{3+}$  which is represented by the black coloured bar in Fig. 11. It is observed that the sensor quantifies the presence of  $\text{Fe}^{3+}$  in all the three samples precisely as shown by the red coloured bar. The detected amount of  $\text{Fe}^{3+}$  is less than the actual amount. Furthermore, to verify the selectivity of the sensor, the same concentration of  $\text{Ca}^{2+}$  is added to each of the samples as interfering ion. In this case, the detected amount of  $\text{Fe}^{3+}$

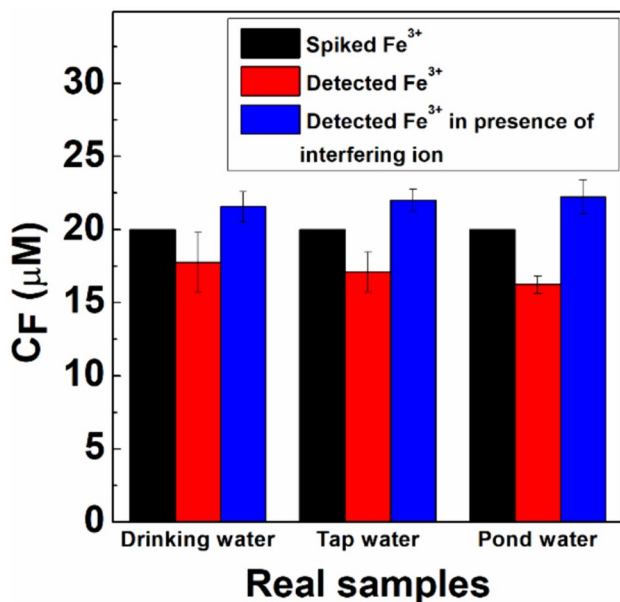


Fig. 11 Comparison of detected concentration of  $\text{Fe}^{3+}$  in real samples

by the sensor is more than the actual amount. These false positive and negative values are shown by optical sensors in several situations where there is an interference due to other ions. For instance, colorimetric detection of  $\text{Pb}^{2+}$  in real samples by label-free gold nanoparticles shows a recovery of 96–103% [55]. Therefore, it can be concluded that AgNPs-based sensor detects approximately actual concentration of the analyte in all the samples even in presence of interfering ion. This proves the remarkable efficiency of the sensor for practical applications.

### Quantitative Detection of $\text{Cu}^{2+}$

The absorption spectra of AgNPs treated with varying concentrations of  $\text{Cu}^{2+}$  ions are depicted in Fig. 12a. A gradual decrease in the absorbance can be observed as the concentration of  $\text{Cu}^{2+}$  ( $C_C$ ) increases from 20 to  $600 \mu\text{M}$ . As the  $C_C$  is increased to  $800 \mu\text{M}$ , the complete disappearance of SPR band takes place which attributes to the loss of stability of AgNPs. There are negligible variations in the SPR position up to the  $C_C$  of  $400 \mu\text{M}$ , and on further increasing the  $C_C$ , there is a red shift followed the disappearance of SPR band. The red shift also suggests the increase in particle size due to decreasing stability of AgNPs. Evaluating the relative change in SPR absorbance of each of these solutions from Fig. 12b, it is clear that the plot converges to a linear fit in the mentioned concentration range. The linear fit follows Eq. (20) with an  $R^2$  value of 0.99;

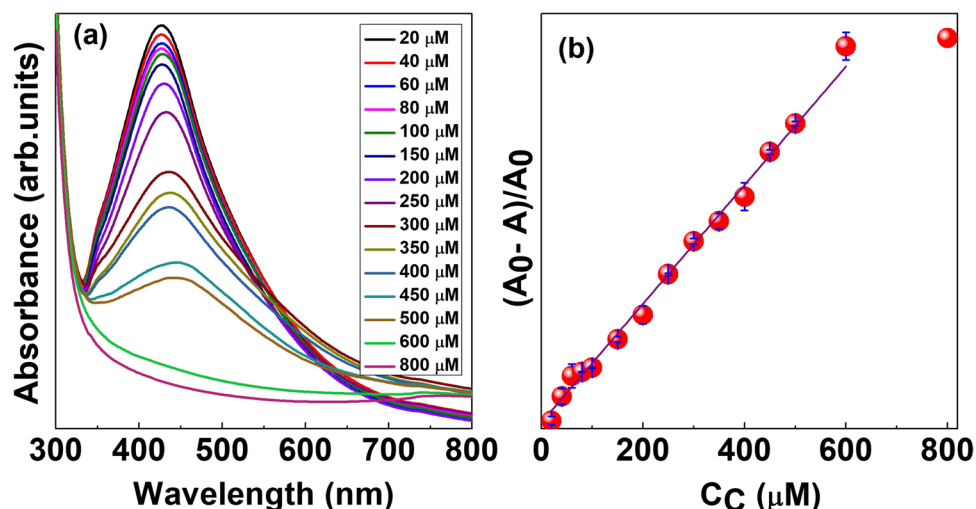
$$\Delta A/A_0 = 0.001C_c - 0.012 \quad (20)$$

The LOD for  $\text{Cu}^{2+}$  detection was obtained as  $19.5 \mu\text{M}$  and the LOQ as  $52.9 \mu\text{M}$ .

### Mechanism

The mechanism of sensing can be explained considering two parameters; one being the affinity of capping agents towards  $\text{Fe}^{3+}$  and  $\text{Cu}^{2+}$  ions and the other is the oxidising ability of these ions in the solution. By the introduction of  $\text{Fe}^{3+}$  and  $\text{Cu}^{2+}$  ions in the AgNP solution, the SPR intensity is decreased. This indicates the reduction of the particular sized AgNPs in the solution. This could be due to the destabilisation of AgNPs since the negatively charged capping agents of leaf extracts show more affinity towards the positively charged  $\text{Fe}^{3+}$  and  $\text{Cu}^{2+}$  ions and thus leaves  $\text{Ag}^0$  to bind with the newly introduced ions. As the concentration of ions increases, the destabilisation rate increases and hence the SPR intensity decreases more and more. When the  $C_F$  and  $C_C$  exceeds a certain limit, say,  $300 \mu\text{M}$  and  $600 \mu\text{M}$  respectively, the ions can easily access the AgNPs and oxidises them to form  $\text{Ag}^+$  ions. This eliminates the AgNPs in

**Fig. 12** **a** Absorption spectra of AgNPs treated with different concentrations of  $\text{Cu}^{2+}$  in  $\mu\text{M}$  and **b** relative change in absorbance with as a function of  $C_C$  showing the linear fit in the entire concentration range excluding 800  $\mu\text{M}$



the solution and is reflected in the absorption spectra with the disappearance of SPR peak.

To substantiate the mechanism, the hydrodynamic size of AgNPs at different concentrations of the analytes and zeta potential of AgNPs before and after the addition of analytes were measured and presented as supplementary information Figs. S1, S2, S3 and S4 respectively. From Figs. S1 and S2, it can be observed that, the uniformity of the hydrodynamic size of AgNPs is lost as the  $C_F$  or  $C_C$  is increased. Furthermore, the spectra shifts towards higher diameters indicating the destabilisation and aggregation of AgNPs that resulted in bigger particles. This is in correlation with the right shift of SPR peak position observed in the UV–visible analysis as shown in Fig. 10a. Furthermore, Figs. S3 and S4 show the zeta potentials measured at  $C_F = 300 \mu\text{M}$  and  $C_C = 600 \mu\text{M}$ . It is clear that the stability of AgNPs is completely lost at these concentrations since the ZP values spike at 0 mV. The ZP values suggest that the negatively charged capping agents present in the leaf extract which were surrounding the AgNPs are no more present surrounding the NPs and hence the negative ZP value is vanished. Thus, the above results explicitly explain the mechanism optical sensing by AgNPs.

The comparison of changes in absorbance of AgNPs with the introduction of  $\text{Fe}^{3+}$  and  $\text{Cu}^{2+}$  ions is shown in Fig. 13. It is clear that the absorbance value decreases non-linearly by the introduction of  $\text{Fe}^{3+}$  and linearly by the introduction of  $\text{Cu}^{2+}$ . The polyphenols present in Tulasi leaves exhibit high affinity towards  $\text{Fe}^{3+}$ , and hence, there is a sudden increase in the relative change in absorbance of AgNPs in the initial stage [32]. Furthermore, the difference in the trends of the relative change in absorbance for  $\text{Fe}^{3+}$  and  $\text{Cu}^{2+}$  can also be attributed to two more factors, one being the higher charge in  $\text{Fe}^{3+}$ , and the second being the lower negative value of cell potential. The higher charge in  $\text{Fe}^{3+}$  compared to  $\text{Cu}^{2+}$  increases the electrostatic affinity of negatively charged capping agents towards  $\text{Fe}^{3+}$  resulting in faster destabilisation of

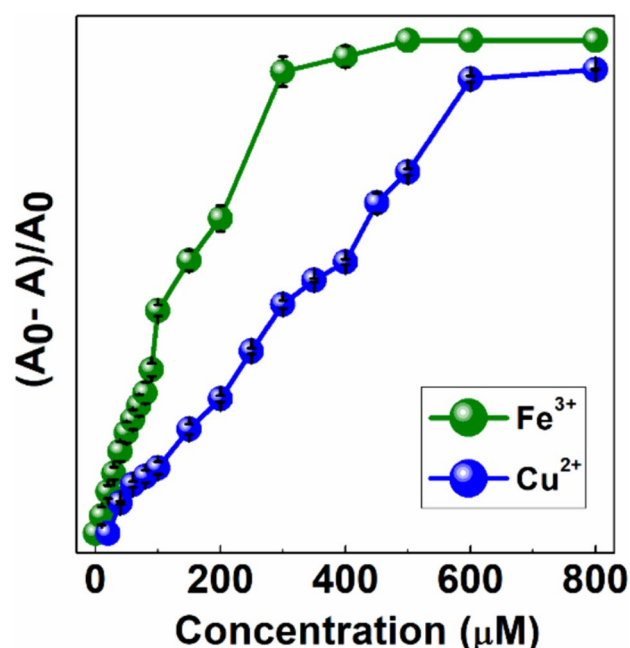


**Fig. 13** Comparison of relative change in absorbance of AgNPs with the introduction of  $\text{Fe}^{3+}$  and  $\text{Cu}^{2+}$  ions

AgNPs. Besides, the lower negative value of Ag/ $\text{Fe}^{3+}$  system when compared to Ag/ $\text{Cu}^{2+}$  system indicates that AgNPs are more vulnerable to oxidation by  $\text{Fe}^{3+}$  than  $\text{Cu}^{2+}$ . Consequently, the relative absorbance changes of both the ions follow two kinetics and hence the difference in the nature of the plots.

### Performance of AgNP-based Paper Sensors

The collected paper punches were successfully covered with AgNPs and images of the papers before and after fabrication is given in Fig. 14a and b. It can be seen that

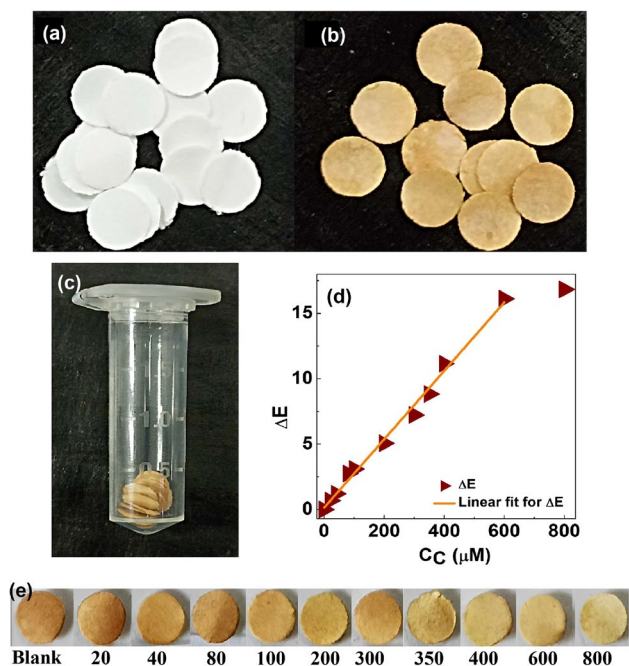


**Fig. 14** **a** The collected paper punches, **b** fabricated paper sensors, **c** paper sensors stored in a vial, **d** variation of  $\Delta E$  parameter as a function of  $C_C$  for sensing with the obtained linear fit and **e** the photographs of paper sensors treated with the  $Cu^{2+}$  solutions of mentioned concentrations (in  $\mu M$ )

value products which are tiny, simple paper sensors are developed out of the waste from the hole punch. These sensors are very easy to carry, store and handle as evident from Fig. 14c showing the sensors being stored in a small vial of 2 mL by volume. Figure 14e depicts the visual readout efficiency of the sensors as the concentration of  $Cu^{2+}$  varies. It can be easily detected by naked eyes that a significant colour change occurs for the sensors with increasing  $C_C$ . The colour changes from the reddish brown

of blank solution to pale yellow and finally turns white. The colour change can be better illustrated by the colour space of dimensions lightness ( $L^*$ ), chroma ( $a^*$ ) and hue ( $b^*$ ). The values are in general called as LAB values and were obtained from the *Adobe photoshop* application. The colour change of any sample from that of the reference can be quantified in terms of  $\Delta E$  parameter which can be expressed as follows [56];

$$\Delta E = \sqrt{(L^* - L_{Blank}^*)^2 + (a^* - a_{Blank}^*)^2 + (b^* - b_{Blank}^*)^2} \tag{21}$$

The values of  $\Delta E$  parameters of the samples are plotted and shown in Fig. 14d. It is evident from the graph that a pronounced and gradual variation is exhibited by the sensors in response to the increase in  $C_C$  which is in agreement with the UV-visible spectra of  $Cu^{2+}$  detection. A linear fit for the plot is obtained satisfying the following expression with  $R^2$  value of 0.99;

$$\Delta E = 0.0267C_C - 0.15205 \tag{22}$$

The calculated LOD is 23.1  $\mu M$  and LOQ is 76  $\mu M$ . The sensitivity of the probes in both the solution from and paper is appreciable when considering the fact that the maximum permissible level of  $Cu^{2+}$  ions in drinking water, according to the World Health Organisation (WHO), is 31.4  $\mu M$  (2 mg/L) [57]. Therefore the sensors exhibit a marked reliability with which they can be used to quantitatively measure the  $Cu^{2+}$  content in aqueous samples.

A comparison table for revealing the merit of this work with already existing sensing probes for  $Fe^{3+}$  and  $Cu^{2+}$  is given in Table 2.

In short, simple, facile and cost-effective sensors are developed by incorporating the benefits of green synthesis and waste valorisation without compromising the efficiency.

**Table 2** Comparison table of present work with previously reported works

Synthesis method	LOD	Range of detection	References
<b>AgNP for <math>Fe^{3+}</math> detection</b>			
Chemical	-	2.4–69 $\mu M$	[58]
Chemical	125.00 $\mu M$	2.5–150 $\mu M$	[52]
Chemical	17.00 $\mu M$	0–10 $\mu M$	[53]
Green, <i>S. arvensis</i> leaf extract	1.00 mM	-	[54]
<b>Green, Tulasi leaf extract</b>	<b>9.10 <math>\mu M</math></b>	<b>0–800 <math>\mu M</math></b>	<b>This work</b>
<b>AgNP for <math>Cu^{2+}</math> detection</b>			
Chemical	0.5 $\mu M$	0.1–10 $\mu M$	[49]
Chemical	100 nM	1–100 $\mu M$	[59]
Chemical	0.1 $\mu M$	0.01–100 $\mu M$	[60]
Chemical	4.3 $\mu M$	6.25–100 $\mu M$	[25]
<b>Green, Tulasi leaf extract</b>	<b>19.5 <math>\mu M</math></b>	<b>0–600 <math>\mu M</math></b>	<b>This work</b>

## Conclusion

In this work, a potential sensor probe is developed using TLE-mediated AgNPs for the detection of  $\text{Fe}^{3+}$  and  $\text{Cu}^{2+}$  ions. The as-synthesised AgNPs exhibit sharp and high SPR absorption at 413 nm and the size of the AgNPs was found to be  $18 \pm 5$  nm. The FTIR spectra evidences for the competent stabilisation of AgNPs by TLE which is reflected in the high ZP value of  $-25.5$  mV. A naked eye detection of  $\text{Fe}^{3+}$  and  $\text{Cu}^{2+}$  from other metal ions was qualitatively achieved along with the spectroscopic evidences. Quantification of  $\text{Fe}^{3+}$  was made possible within a wide nonlinear range of  $0\text{--}800$   $\mu\text{M}$  and the detection limit extends up to  $9.1$   $\mu\text{M}$ , whereas in the case of  $\text{Cu}^{2+}$ , the LOD is obtained as  $19.5$   $\mu\text{M}$  in the linear range of  $0\text{--}600$   $\mu\text{M}$ . The explained sensing mechanism of aggregation and reduction potentials is substantiated by experimental and theoretical evidences effectively. In addition, an extraordinarily simple paper sensors were developed for the detection of  $\text{Cu}^{2+}$  ions and successively quantified the colorimetric response using LAB values and  $\Delta E$  parameter with a LOD of  $23.1$   $\mu\text{M}$ . The work presents a novel, economic and eco-friendly sensor probe which has very high sensitivity and selectivity towards the analytes tested and can be considered a tiny step towards waste valorisation.

**Supplementary Information** The online version contains supplementary material available at <https://doi.org/10.1007/s11468-024-02431-0>.

**Author Contribution** All the authors contributed to the study conception and design. R. R performed sample preparation, data collection, analysis and the drafting of manuscript. K. C. S. supervised the work. All authors read and approved the final manuscript.

**Funding** This work is supported by the project (03/1485/2023/EMR-II), funded by Council for Scientific and Industrial Research, (03/1485/23/EMR-II) and UGC (F.4-5(59)/2014(BSR) (FRP)), Govt. of India.

**Data Availability** No datasets were generated or analysed during the current study.

## Declarations

**Ethical Approval** This declaration is not applicable.

**Competing Interests** The authors declare no competing interests.

## References

- Crans DC, Kostenkova K (2020) Open questions on the biological roles of first-row transition metals. *Commun Chem* 3:104
- Tagliabue A, Bowie AR, Boyd PW, Buck KN, Johnson KS, Saito MA (2017) The integral role of iron in ocean biogeochemistry. *Nature* 543:51–59
- Semeniuk DM, Bundy RM, Payne CD, Barbeau KA, Maldonado MT (2015) Acquisition of organically complexed copper by marine phytoplankton and bacteria in the northeast subarctic Pacific Ocean. *Mar Chem* 173:222–233
- Festa RA, Thiele DJ (2011) Copper: an essential metal in biology. *Curr Biol* 21:R877–R883
- Lasocki S, Longrois D, Montravers P, Beaumont C, Riou B (2011) Hepcidin and anemia of the critically ill patient. *Anesthesiology* 114:688–694
- Mir AR, Pichtel J, Hayat S (2021) Copper: uptake, toxicity and tolerance in plants and management of Cu-contaminated soil. *Biometals* 34:737–759
- Lutsenko S (2020) Sending copper where it is needed most. *Science* 368:584–585
- Wang P, Yuan Y, Xu K, Zhong H, Yang Y, Jin S, Yang K, Qi X (2021) Biological applications of copper-containing materials. *Bioact Mater* 6:916–927
- Lieu PT, Heiskala M, Peterson PA, Yang Y (2001) The roles of iron in health and disease. *Mol Aspects Med* 22:1–87
- Laglera LM, Monticelli D (2017) Iron detection and speciation in natural waters by electrochemical techniques: a critical review. *Curr Opin Electrochem* 3:123–129
- Malik LA, Bashir A, Qureshi A, Pandith AH (2019) Detection and removal of heavy metal ions: a review. *Environ Chem Lett* 17:1495–1521
- Ali S, Chen X, Shi W, Huang G, Yuan L, Meng L, Chen S, Zhonghao X, Chen X (2023) Recent advances in silver and gold nanoparticles-based colorimetric sensors for heavy metal ions detection: a review. *Crit Rev Anal Chem* 53:718–750
- Do Dat T, Cong CQ, Le Hoai NT, Khang PT, Nam NTH, Thi Tinh N, Hue DT, Hieu NH (2023) Green synthesis of gold nanoparticles using *Andrographis paniculata* leave extract for lead ion detection, degradation of dyes, and bioactivities. *Biochem Eng J* 200:109103
- Jayeoye TJ, Sirimahachai U, Wattanasin P, Rujiralai T (2022) Eco-friendly poly(aniline boronic acid)/gum tragacanth stabilized silver nanoparticles nanocomposite for selective sensing of  $\text{Hg}^{2+}$ . *Microchem J* 182:107949
- Farhadi K, Forough M, Molaei R, Hajizadeh S, Rafipour A (2012) Highly selective  $\text{Hg}^{2+}$  colorimetric sensor using green synthesized and unmodified silver nanoparticles. *Sens Actuators B Chem* 161:880–885
- Eze FN, Jayeoye TJ, Tola AJ (2021) Fabrication of label-free and eco-friendly ROS optical sensor with potent antioxidant properties for sensitive hydrogen peroxide detection in human plasma. *Colloids Surf B Biointerfaces* 204:111798
- Dat NM, Cong CQ, Hai ND et al (2023) Facile synthesis of eco-friendly silver@graphene oxide nanocomposite for optical sensing. *ChemistrySelect* 8:e202204183
- Li Z, Ti M, Yang K, Li X, Wu L, He Y (2019) Colorimetric detection of iron (II) using 4-mercaptobenzoic acid and 3,3',5,5'-tetramethylbenzidine modified silver nanoparticles. *Microchem J* 151:104254
- Jayeoye TJ, Eze FN, Olatunji OJ, Tyopine AA (2022) Synthesis of biocompatible Konjac glucomannan stabilized silver nanoparticles, with *Asystasia gangetica* phenolic extract for colorimetric detection of mercury (II) ion. *Sci Rep* 12:9176
- Gao X, Lu Y, He S, Li X, Chen W (2015) Colorimetric detection of iron ions (III) based on the highly sensitive plasmonic response of the N-acetyl-L-cysteine-stabilized silver nanoparticles. *Anal Chim Acta* 879:118–125
- Jayeoye TJ, Eze FN, Muangsin N (2023) An innovative synthesis of (Ag<sub>0</sub>-pullulan-Ag<sup>+</sup>) as an optical nanoprobe for sensitive and selective detection of  $\text{Fe}^{2+}$  ion based on redox reaction. *Mater Today Chem* 32:101637
- Doan VD, Phan TL, Le VT, Vasseghian Y, Evgenievna LO, Tran DL, Le VT (2022) Efficient and fast degradation of

- 4-nitrophenol and detection of Fe(III) ions by *Poria cocos* extract stabilized silver nanoparticles. *Chemosphere* 286:131894
23. Ratnarathorn N, Chailapakul O, Henry CS, Dungchai W (2012) Simple silver nanoparticle colorimetric sensing for copper by paper-based devices. *Talanta* 99:552–557
  24. Retno Yuniarni D, Intan Pratiwi N, Umar A, Imawan C (2020) Synthesis of silver nanoparticles (AgNPs) using sodium chloride (NaCl) for iron (III) ions detection based on colorimetric and optical changes. *J Phys Conf Ser* 1528:012062
  25. Teeparuksapun K, Prasongchan N, Thawonsuwan A (2019) Alpha-lipoic acid functionalized silver nanoparticles for colorimetric detection of copper ion. *Anal Sci* 35:371–377
  26. Lopez ECR, Zafra MA, Gavan JNL, Villena EDA, Almaquer FEP, Perez JVD (2020) Humic acid functionalized - silver nanoparticles as nanosensor for colorimetric detection of copper (II) ions in aqueous solutions. *Key Eng Mater* 831:142–150
  27. Nam NTH, Linh NTT, Dat NM, Bao PP, Tinh NT, Cong CQ, Hai ND, Giang NTH, Phong MT, Hieu NH (2023) Applications of highly stable silver nanoparticles from *Garcinia mangostana* pericarp extract: bioactivities, catalysis, and optical sensing. *ChemistrySelect* 8:e202301602
  28. Hai ND, Dat NM, Huong LM, Tai LT, Thinh DB, Nam NTH, Dat NT, Phong MT, Hieu NH (2022) Phytosynthesis of silver nanoparticles using *Mangifera indica* leaves extract at room temperature: formation mechanism, catalytic reduction, colorimetric sensing, and antimicrobial activity. *Colloids Surf B Biointerfaces* 220:112974
  29. Nam NTH, Dat NM, Hai ND et al (2023) Green synthesis of silver@graphene oxide nanocomposite for antibacterial, cytotoxicity assessment, and hydrogen peroxide electro-sensing. *New J Chem* 47:8090–8101
  30. Baruah K, Haque M, Langbang L, Das S, Aguan K, Singha Roy A (2021) *Ocimum sanctum* mediated green synthesis of silver nanoparticles: a biophysical study towards lysozyme binding and anti-bacterial activity. *J Mol Liq* 337:116422
  31. Singh AK (2022) *Ocimum sanctum* mediated phytosynthesis of metallic nanoparticles: a review. *Bioresour Technol Rep* 19:101118
  32. Perron NR, Brumaghim JL (2009) A review of the antioxidant mechanisms of polyphenol compounds related to iron binding. *Cell Biochem Biophys* 53:75–100
  33. Chaudhary A, Sharma S, Mittal A, Gupta S, Dua A (2020) Phytochemical and antioxidant profiling of *Ocimum sanctum*. *J Food Sci Technol* 57:3852–3863
  34. Rugmini R, Sekhar KC, Sathish S (2024) Synthesis of silver nanoparticles for photothermal and sensing applications and sustainable gel formation. *Mater Res Innov* 28:278–287
  35. Jain S, Mehata MS (2017) Medicinal plant leaf extract and pure flavonoid mediated green synthesis of silver nanoparticles and their enhanced antibacterial property. *Sci Rep* 7:15867
  36. Dubey SP, Lahtinen M, Särkkä H, Sillanpää M (2010) Bioprospective of *Sorbus aucuparia* leaf extract in development of silver and gold nanocolloids. *Colloids Surf B Biointerfaces* 80:26–33
  37. Badr Y, Wahed MGAE, Mahmoud MA (2006) On 308nm photofragmentation of the silver nanoparticles. *Appl Surf Sci* 253:2502–2507
  38. Debnath S, Swetha D, Babu MN (2020) Green synthesis of nanoparticles using herbal extract. In: Sen S, Chakraborty R (eds) *Herb. Med. India*. Springer Singapore, Singapore, pp 205–213
  39. Amin M, Anwar F, Janjua MRSA, Iqbal MA, Rashid U (2012) Green synthesis of silver nanoparticles through reduction with *Solanum xanthocarpum* L. berry extract: characterization, antimicrobial and urease inhibitory activities against *Helicobacter pylori*. *Int J Mol Sci* 13:9923–9941
  40. Kumar R, Roopan SM, Prabhakarn A, Khanna VG, Chakraborty S (2012) Agricultural waste *Annona squamosa* peel extract: biosynthesis of silver nanoparticles. *Spectrochim Acta A Mol Biomol Spectrosc* 90:173–176
  41. Adur AJ, Nandini N, Shilpashree Mayachar K, Ramya R, Srinatha N (2018) Bio-synthesis and antimicrobial activity of silver nanoparticles using anaerobically digested parthenium slurry. *J Photochem Photobiol B* 183:30–34
  42. Singhal G, Bhavesh R, Kasariya K, Sharma AR, Singh RP (2011) Biosynthesis of silver nanoparticles using *Ocimum sanctum* (Tulsi) leaf extract and screening its antimicrobial activity. *J Nanoparticle Res* 13:2981–2988
  43. Jaffar SS, Saallah S, Misson M, Siddiquee S, Roslan J, Lenggoro W (2023) Green synthesis of flower-like carrageenan-silver nanoparticles and elucidation of its physicochemical and antibacterial properties. *Molecules* 28:907
  44. Gumustas M, Sengel-Turk CT, Gumustas A, Ozkan SA, Uslu B (2017) Effect of polymer-based nanoparticles on the assay of antimicrobial drug delivery systems. *Multifunct Syst Comb Deliv Biosensing Diagn*. Elsevier, pp 67–108
  45. Singh J, Kumar S, Dhaliwal AS (2021) Green synthesis of silver nanoparticles using *Ocimum tenuiflorum* leaf extract: characterization, antioxidant and catalytic activity. Longowal, India, p 040017
  46. Bagur H, Poojari CC, Melappa G, Rangappa R, Chandrasekhar N, Somu P (2020) Biogenically synthesized silver nanoparticles using endophyte fungal extract of *Ocimum tenuiflorum* and evaluation of biomedical properties. *J Clust Sci* 31:1241–1255
  47. Singh J, Mehta A, Rawat M, Basu S (2018) Green synthesis of silver nanoparticles using sun dried tulsi leaves and its catalytic application for 4-Nitrophenol reduction. *J Environ Chem Eng* 6:1468–1474
  48. Uzunoğlu D, Ergüt M, Kodaman CG, Özer A (2020) Bio-synthesized silver nanoparticles for colorimetric detection of Fe<sup>3+</sup> ions. *Arab J Sci Eng*. <https://doi.org/10.1007/s13369-020-04760-8>
  49. Miao LJ, Xin JW, Shen ZY, Zhang YJ, Wang HY, Wu AG (2013) Exploring a new rapid colorimetric detection method of Cu<sup>2+</sup> with high sensitivity and selectivity. *Sens Actuators B Chem* 176:906–912
  50. Haynes WM, Lide DR, Bruno TJ (eds) (2016) *CRC Handbook of Chemistry and Physics*, 97th ed. <https://doi.org/10.1201/9781315380476>
  51. Zou R, Guo X, Yang J, Li D, Peng F, Zhang L, Wang H, Yu H (2009) Selective etching of gold nanorods by ferric chloride at room temperature. *CrystEngComm* 11:2797
  52. Zhan J, Wen L, Miao F, Tian D, Zhu X, Li H (2012) Synthesis of a pyridyl-appended calix[4]arene and its application to the modification of silver nanoparticles as an Fe<sup>3+</sup> colorimetric sensor. *New J Chem* 36:656–661
  53. Coutinho MS, Latocheski E, Neri JM, Neves ACO, Domingos JB, Cavalcanti LN, Gasparotto LHS, Moraes EP, Menezes FG (2019) Rutin-modified silver nanoparticles as a chromogenic probe for the selective detection of Fe<sup>3+</sup> in aqueous medium. *RSC Adv* 9:30007–30011
  54. Chandraker SK, Ghosh MK, Lal M, Ghorai TK, Shukla R (2019) Colorimetric sensing of Fe<sup>3+</sup> and Hg<sup>2+</sup> and photocatalytic activity of green synthesized silver nanoparticles from the leaf extract of *Sonchus arvensis* L. *New J Chem* 43:18175–18183
  55. Hung YL, Hsiung TM, Chen YY, Huang YF, Huang CC (2010) Colorimetric detection of heavy metal ions using label-free gold nanoparticles and alkanethiols. *J Phys Chem C* 114:16329–16334
  56. Castillo PM, Fernández-Acejo FJ, Carnerero JM, Prado-Gotor R, Jimenez-Ruiz A (2021) Colorimetric, naked-eye detection of lysozyme in human urine with gold nanoparticles. *Nanomaterials* 11:612
  57. Awad FS, AbouZied KM, Bakry AM, Abou El-Maaty WM, El-Wakil AM, El-Shall MS (2020) Highly fluorescent hematoporphyrin modified graphene oxide for selective detection of copper ions in aqueous solutions. *Anal Chim Acta* 1140:111–121

58. Bothra S, Solanki JN, Sahoo SK, Callan JF (2014) Anion-driven selective colorimetric detection of Hg<sup>2+</sup> and Fe<sup>3+</sup> using functionalized silver nanoparticles. *RSC Adv* 4:1341–1346
59. Zhang Z, Zhao W, Hu C, Guo D, Liu Y (2022) Colorimetric copper (II) ions detection in aqueous solution based on the system of 3'3'5'5'-tetramethylbenzidine and AgNPs in the presence of Na<sub>2</sub>S<sub>2</sub>O<sub>3</sub>. *J Sci Adv Mater Devices* 7:100420
60. Jeevika A, Ravi Shankaran D (2014) Visual colorimetric sensing of copper ions based on reproducible gelatin functionalized silver nanoparticles and gelatin hydrogels. *Colloids Surf Physicochem Eng Asp* 461:240–247

**Publisher's Note** Springer Nature remains neutral with regard to jurisdictional claims in published maps and institutional affiliations.

Springer Nature or its licensor (e.g. a society or other partner) holds exclusive rights to this article under a publishing agreement with the author(s) or other rightsholder(s); author self-archiving of the accepted manuscript version of this article is solely governed by the terms of such publishing agreement and applicable law.